https://doi.org/10.5194/egusphere-2026-6048
Preprint. Discussion started: 17 November 2026
© Author(s) 2026. CC BY 4.0 License.

Validation of SPEXone aerosol products using PACE-PAX campaign data

Jasper Mens[1], Martijn Smit[1], Brecht Simon[1], Guangliang Fu[1], Otto Hasekamp[1], Brian Cairns[2], Joseph Schlosser[3], and Bastiaan van Diedenhoven[1]

[1]SRON Space Research Organisation Netherlands, Niels Bohrweg 4, 2333 CA Leiden, The Netherlands
[2]NASA Goddard Institute for Space Studies, 545 West 112th St New York, NY 00125, United States
[3]Hampton University, Department of Chemical Engineering, 168 Marshall Ave., Franklin W. Olin Engineering Building, Hampton, VA 23668, United States

Correspondence: Jasper Mens (j.h.mens@sron.nl)

Abstract.

In September 2024, six months after the launch of the Plankton Aerosol Cloud and ocean Ecosystem (PACE) satellite, the PACE Postlaunch Airborne eXperiment (PACE-PAX) campaign was conducted in southern California. Using a wide array of instruments, including airborne proxies to satellite instruments, the stated goal of the campaign was to validate satellite data products from both PACE and EarthCARE. As part of the campaign, SPEX airborne, the predecessor of SPEXone on PACE, was operated from NASA's high-altitude ER-2 aircraft, producing a large number of collocated observations with a wide-ranging suite of other instruments.

The main objective of this paper is to use the rich dataset produced by this campaign to evaluate the quality of aerosol retrievals from SPEXone. We begin by comparing the radio-polarimetric measurements from SPEXone and SPEX airborne to those from the reference polarimeter RSP, which was operated alongside SPEX airborne. We find that the radiance and polarisation data from the three polarimeters are broadly consistent with each other, and free of unexpected systematic differences.

We evaluate the performance of the SPEX airborne aerosol retrievals, obtained using the same version of the RemoTAP algorithm that was used for SPEXone, through comparisons to AERONET and airborne in situ measurements. We find that SPEX airborne performs well against AERONET in terms of the AOD and Angström exponent, with a Root-Mean-Square Deviation (RMSD) of 0.05 and 0.32 respectively (with $AOD_{532}>0.1$). The SSA lags behind somewhat, with an RMSD of 0.05, which we attribute to the low AOD throughout the campaign. Evaluating the volume water fraction, effective radius, and number concentration against airborne in situ measurements, we again find good agreement in the former two, but a notable overestimation in the number concentration over land. Finally, we directly compare the collocated retrievals from SPEX airborne and SPEXone for each of the parameters discussed above. Although limited by the quantity and diversity of data, we find good agreement in the majority of cases, concluding that SPEX airborne is a good proxy for SPEXone.

https://doi.org/10.5194/egusphere-2026-6048
Preprint. Discussion started: 17 November 2026
© Author(s) 2026. CC BY 4.0 License.

1 Introduction

SPEXone, the Dutch spectro-polarimeter instrument designed to observe and characterize atmospheric aerosol has been making continuous observations on NASA's Plankton Aerosol Cloud and ocean Ecosystem (PACE) satellite (Werdell et al., 2019; Amerongen et al., 2019; Rietjens, 2020; Hasekamp et al., 2019) since its launch in February 2024. These first years of operation have seen significant efforts toward the calibration and validation of the instrument, with an important component being comparisons to established ground-based reference instruments. For SPEXone, however, this is comparatively challenging; due to its narrow ground swath, consecutive observations of a location can be a month or more apart, so the ability to gather a sufficiently large sample of collocated observations hinges on a high spatial (and temporal) density of ground-based measurements. This effectively leaves the Aerosol Robotic Network (AERONET) as the only viable option, and, while the results of these comparisons are impressive (Fu et al., 2025, 2026), the SPEXone retrievals include many more aerosol properties than AERONET provides. To supplement these comparisons, then, dedicated airborne campaign data is invaluable. By operating a remote sensing instrument from a high-altitude aircraft instead of a satellite, the flight path can be planned around targeted observations of ground-based and airborne instruments, and reference instruments can be operated from the same platform. The resulting dataset of collocated observations provides a far more complete insight into the performance of the instrument, and allow for a more extensive evaluation of its performance.

Of course, operating from an aircraft comes with its own set of design requirements, and a perfect copy of the instrument is usually not available, so instead these campaigns work with airborne proxy instruments. As a proxy for SPEXone, we use its predecessor: SPEX airborne (Smit et al., 2019). While there are some differences between these two instruments, they operate on the same principles; both instruments provide observations of atmospheric aerosols through hyperspectral radio-polarimetric measurements at multiple angles (Snik et al., 2009), with the most notable difference between the two being that SPEX airborne has nine viewing angles, compared to SPEXone's five. Being the predecessor to SPEXone, SPEX airborne had already been deployed in campaigns prior to the launch of PACE, such as the ACEPOL campaign in 2018 (Knobelspiesse et al., 2020), where it was operated alongside airMSPI (Diner et al., 2013) and the Research Scanning Polarimeter (RSP) (Cairns et al., 1999). This allowed for inter-instrument comparisons of the radio-polarimetric measurements (Smit et al., 2019), as well as the resulting aerosol products (Fu et al., 2020), both of which found excellent performance, paving the way for the eventual deployment of SPEXone on PACE. Despite the similarities between SPEX airborne and SPEXone, however, conclusions about the performance of the former cannot necessarily be extended to the performance of the latter. A validation of SPEXone, then, required a new campaign, wherein the two instruments can be compared directly.

The PACE Postlaunch Airborne eXperiment (PACE-PAX) campaign took place in September 2024 around the southwestern coast of the United States (Knobelspiesse et al., 2025b, 2026). The goal of this campaign was to validate a large and disparate set of satellite observations from PACE, as well as the European Space Agency's EarthCARE (Wehr et al., 2023). The objectives ranged from marine phytoplankton concentrations to aerosol properties and cloud droplet size distributions, and to this end the campaign involved extensive coordination between a varied ensemble of measurement platforms. Pivotal to the campaign was NASA's ER-2 high-altitude aircraft carrying a suite of six airborne proxies to PACE and EarthCARE instruments, among

https://doi.org/10.5194/egusphere-2026-6048
Preprint. Discussion started: 17 November 2026
© Author(s) 2026. CC BY 4.0 License.

which were RSP and SPEX airborne. Over the course of the deployment the ER-2 amassed a total of 81 flight hours across 13 science flights. These flights were carefully planned to produce collocated observations with AERONET stations, as well as extended observations overlapping the PACE and EarthCARE ground tracks during overpasses. Equally important, however, were collocated observations with the other mobile observation platforms participating in the campaign, including a Twin Otter propeller aircraft equipped with aerosol sampling instrumentation, operated by the Center for Interdisciplinary Remotely Piloted Aircraft Studies (CIRPAS).

In this paper we leverage the large set of collocated observations produced by the PACE-PAX campaign to evaluate the performance of SPEXone. We begin with a qualitative assessment of the radiometric and polarimetric (i.e., level 1) performance of SPEX airborne and SPEXone, comparing each to RSP and finally to each other. We then move to the resulting (level 2) aerosol products, evaluating the performance of SPEX airborne against AERONET measurements of the Aerosol Optical Depth (AOD), Ångström exponent (AE), and Single Scattering Albedo (SSA). We additionally evaluate the retrieved volume water fraction (f_w), fine-mode effective radius (r_{eff}^f), and fine-mode number concentration (N_c^f) using the in situ measurements from aboard the Twin Otter. Finally, we evaluate the agreement between SPEX airborne and SPEXone during the extended underflights of the PACE ground track by the ER-2.

This paper is organised as follows: section 2 details the calibration and operation of SPEX airborne as well as the collocation methodology for the aerosol product comparisons. In Sect. 3 we show and discuss both the radio-polarimetric validation and the results of the aerosol product comparisons, and we summarize our conclusions in Sect. 4.

2 Data & Methods

2.1 SPEX airborne data acquisition and processing

SPEX airborne (Smit et al., 2019) provides measurements from nine viewing directions, nominally aligned with the ground-track. The viewing directions are spaced uniformly across the total viewing range of -56°to +56°, and data are sampled for each viewing angle in push-broom mode. With each viewing angle having an across-track angular width of approximately 7°, the projected swath on ground varies from ~2.4 km at Nadir to ~4.3 km at the outermost viewing angles when operating from the ER-2 at a cruising altitude of 20 km. SPEX airborne is designed to provide an instantaneous Field Of View (iFOV) of one square degree (about 350×350 m Nadir). Spectra are captured in the focal plane with a 2072×2072 pixel CCD sensor, where the 7° swath is oversampled with ~60 pixels. This allows for geolocation with an accuracy down to 0.1° (about 35 m), which is achieved via postprocessing by analysing the pushbroom imagery at the highest available spatial resolution to identify and correct for possible misalignments (details of the precise procedure can be found in van der Schaaf et al. (2024)). Like in the ACEPOL campaign, SPEX airborne was mounted in the right wingpod of the ER-2 aircraft with tailnumber "809". Throughout each flight, as fuel is consumed, the wings of the ER-2 slowly flex, slightly changing the viewing direction of the instruments mounted in the wingpods. We account for this process with an analytical model.

To achieve an adequate SNR, SPEX airborne data are sampled with an effective exposure time of 1.75 seconds, which leads to 364 m along-track sampling at the ER-2 cruise speed of 208 m s^{-1}. Geolocated radiance and polarimetric data from the nine

https://doi.org/10.5194/egusphere-2026-6048
Preprint. Discussion started: 17 November 2026
© Author(s) 2026. CC BY 4.0 License.

Table 1. Instrument specifications of SPEXone, SPEX airborne and Research Scanning Polarimeter (RSP). [a]: RSP L1C is a 1D grid without a fixed cell dimension. On average, L1C geolocated positions are separated by ~0.2 km

	SPEXone	SPEX airborne	RSP
Viewing angles	$\pm 58°$, $\pm 20°$, $0°$	$\pm 56°$, $\pm 42°$, $\pm 28°$, $\pm 14°$, $0°$	$-63°$ to $+43°$ ($0.8°$ sampling)
Spectral range	385-770 nm	400-760 nm	410-2250 nm
Spectral sampling	2 nm (Rad) / 10-30 nm (DoLP)	2-5 nm (Rad) / 10-40 nm (DoLP)	410, 470, 555, 670, 865, 960, 1590, 1880, 2250 nm
Nadir L1C cell size	5.2×5.2 km^2	1×1 km^2	~0.2 km^2
DoLP accuracy	0.003	0.004-0.005	0.002
Radiance accuracy	2 %	2-4 %	3 %

viewing angles are combined to a common grid of 1×1 km^2 as the L1C product, resulting in a swath that is just a few ground-pixels wide. The effective spectral range of SPEX airborne is 400-760 nm. Note that hyperspectral radiometric and polarimetric data have different spectral resolutions. However, in L1C the radiometric data are also provided on the polarimetric spectral grid, which is used for the aerosol retrievals (see Sect. 2.2).

In many ways the operation and data acquisition of SPEX airborne during PACE-PAX was identical to that during the ACE-POL campaign, and we refer to Smit et al. (2019) for details about instrument calibration, operation and data processing. The SPEX airborne flight configuration did, however, see some changes since previous deployments: the Single Board Computer was replaced after it had crashed on an earlier fight campaign, the real-time Linux operating system was upgraded, and several safety checks were adapted to higher tolerance to avoid repetitive rebooting of the instrument during flights.

Prior to the PACE-PAX campaign, SPEX airborne was fully re-calibrated with the in-house equipment that was also used in the calibration of SPEXone. This included calibration measurements outlined in Smit et al. (2019), i.e.: line-of-sight calibration, wavelength calibration, and radiometric and polarimetric calibration. The line-of-sight calibration was conducted using a collimated white light source with known beam direction relative to a lab-based reference, while the orientation of SPEX airborne was determined by using theodolites to measure the orientation of a reference cube attached to the instrument relative to the lab-reference. This is the same procedure as followed for SPEXone, as described in Campo et al. (2025) and Rietjens et al. (2023). Radiometric calibration measurements were performed at ESA's European Space Research and Technology Centre (ESTEC), with a setup very similar to the one used for SPEXone: A 12" integrating sphere from Labsphere with a 4" output port diameter, in combination with 150 W halogen lamp. Polarization calibration and demodulation was also modified, and now follows Smit et al. (2021), using parametrised spline prescriptions for normalized Stokes parameters $q(\lambda) = Q/I$ and $u = U/I(\lambda)$ using Mueller matrix elements determined at the spectral resolution of spectral radiance $I(\lambda)$. This same demodulation approach is used for SPEXone. To facilitate easy processing from L1C to L2, we keep the format of the L1C netcdf files identical to that of SPEXone (and its fellow PACE instruments).

https://doi.org/10.5194/egusphere-2026-6048
Preprint. Discussion started: 17 November 2026
© Author(s) 2026. CC BY 4.0 License.

2.2 RemoTAP on SPEX airborne

The level 2 aerosol retrievals for SPEX airborne are processed in the same way as for SPEXone: using the Remote sensing of Trace gas and Aerosol Products (RemoTAP) algorithm (Fan et al., 2019; Fu et al., 2020; Fu and Hasekamp, 2018; Hasekamp et al., 2011, 2024; Lu et al., 2022) developed at SRON Space Research Organisation Netherlands. This algorithm works by fitting a radiative transfer model to multi-angle polarimeter measurements of the radiance and DoLP, taking advantage of the high information content to simultaneously retrieve a large number of aerosol parameters.

The retrievals are split into three modes: fine spherical, coarse spherical (hydrated sea salt), and coarse non-spherical (dust). Each mode is represented with a log-normal size distribution where the effective radius and variance are retrieved parameters. The vertical profile of the aerosols is parametrised as a Gaussian with a full width at half-maximum of 2 km, and a mean height which is retrieved as the Aerosol Layer Height (ALH), defined relative to the surface. The dimensionless parameter χ^2 represents the fit residuals between the forward model and the observations. It is provided with the retrievals for each ground pixel, and should be used to mask out cloud-contaminated or otherwise problematic retrievals. An appropriate maximum for this χ^2 is determined heuristically to strike a balance between the quality and quantity of accepted retrievals, and for this SPEX airborne dataset we use and recommend a threshold of $\chi^2 < 1.5$ over land, and $\chi^2 < 2$ over ocean. One limitation of this dataset is that the processing does not include a dedicated cloud filtering step, which means that this χ^2 filter is the only available mechanism for filtering for clouds. As a result, some cloud-contamination is likely to remain in the dataset.

Because the lowest radiance wavebands tend to suffer from a low SNR, the spectral range of the instrument is slightly truncated before further processing. For this dataset we find the best performance when starting from the 413 nm band.

2.3 SPEX airborne versus AERONET

AERONET stations were important observation targets during the campaign, with the 81 ER-2 flight hours providing around 100 collocated observations with SPEX airborne. We use these observations to validate the Aerosol Optical Depth at 532 nm (AOD_{532}), the 440-670 Ångström exponent ($AE_{440\text{-}670}$), and the Single Scattering Albedo at 440 nm (SSA_{440}). We use the AERONET V3 direct-sun and almucantar inversion data at level 1.5, which are cloud-screened but not quality-assured. When an AOD measurement is not provided at 532 nm, we interpolate between the measurements at the two nearest wavelengths on a log-log scale.

For each SPEX airborne-AERONET collocation, we average the AERONET AOD and Ångström exponent within $\pm$ 1 hour of the moment of closest approach by the ER-2. For the SSA, we extend this window to $\pm$3 hours. As the corresponding SPEX airborne measurement we take the mean of all SPEX airborne data within a radius of 20 km of the AERONET site, and within five minutes of the moment of closest approach. For retrievals over ocean we extend this radius to 30 km, as the conditions over ocean tend to be more uniform than over land.

Because aerosol retrievals are less reliable when AOD is low, we only consider AE and SSA measurements during overpasses with a mean AOD_{532} above 0.1 for both SPEX airborne and AERONET. We additionally exclude collocations with fewer than 10 valid SPEX airborne ground pixels after filtering for χ^2.

https://doi.org/10.5194/egusphere-2026-6048
Preprint. Discussion started: 17 November 2026
© Author(s) 2026. CC BY 4.0 License.

2.4 SPEX airborne versus Twin Otter

We validate the SPEX airborne retrievals of the volume water fraction, fine mode effective radius, and fine mode number concentration against situ measurements from instruments aboard the CIRPAS Twin Otter aircraft, including facility instruments and those operated by the Langley Aerosol Research Group Experiment (LARGE). These data have been processed and prepared using the In Situ Aerosol Retrieval Algorithm (ISARA, Schlosser et al. (2025)), which has the stated goal of closing the gap between in situ measurements and remote sensing estimates by stitching together different size ranges, and correcting for the difference between the humidity within the instrument and ambient conditions. For our purposes, this humidification is really only important for the effective radius comparison, but for the sake of consistency and simplicity we make use of this dataset for the f_w and N^f comparisons as well.

2.4.1 Volume Water Fraction

Our method of computing the volume water fraction, both for the in situ measurements and the remote sensing products, draws heavily from van Diedenhoven et al. (2022). We provide an overview of the methodology, but direct the reader to this existing work for a more detailed treatment of the underlying theory.

The RemoTAP retrieval of f_w is based on the retrieved real refractive index n, as described in Schuster et al. (2009). In summary, this is justified by two assumptions: first, that the real refractive index of a mixed aerosol (n_{mix}) follows the volume mixing rule (i.e., it is the volume-weighted mean of its components' refractive indices), and second, that the real refractive index for dry material (n_{dry}) can be averaged to a single value. Based on previous studies of dry aerosols this average is 1.54, with a standard-deviation (inter-quartile range) of 0.02 (0.04). Given that the real refractive index for water is well-established ($n_{\mathrm{water}} = 1.33$ at 555 nm (Daimon and Masumura, 2007)), a volume water fraction can then be obtained through linear interpolation between these two extremes:

$$f_w = \frac{n_{\mathrm{dry}} - n_{\mathrm{mix}}}{n_{\mathrm{dry}} - n_{\mathrm{water}}}. \tag{1}$$

Note that within RemoTAP the real refractive index is retrieved separately for each mode (and held fixed at 1.53 for non-spherical coarse mode). The total f_w computed using the average of these refractive indices, weighted by the retrieved volume density for each mode.

The corresponding in situ estimate is obtained using humidified nephelometry measurements of the hygroscopic scattering enhancement (cf. van Diedenhoven et al., 2022), which are then related to a volume growth factor and a hygroscopicity parameter.

It is instructive to start at the final step: we begin by expressing f_w in terms of the hygroscopic volume growth factor g_V, representing the fractional difference in particle volume between dry ($\mathrm{RH} = 0\ \%$) to humidified ($\mathrm{RH} > 0\ \%$) conditions:

$$f_w = \frac{g_V(\mathrm{RH}) - 1}{g_V(\mathrm{RH})}. \tag{2}$$

This growth factor can be parametrised by κ-Köhler theory (Petters and Kreidenweis, 2007), which abstracts the ensemble of factors governing hygroscopicity (composition, mixing state, age, etc.) into a single dimensionless parameter κ. In sub-

https://doi.org/10.5194/egusphere-2026-6048
Preprint. Discussion started: 17 November 2026
© Author(s) 2026. CC BY 4.0 License.

saturated conditions, we can approximate g_V as a function of this κ and RH, after Brock et al. (2016):

$$g_V(\mathrm{RH}) \approx 1 + \kappa \left(\frac{\mathrm{RH}}{1 - \mathrm{RH}} \right). \tag{3}$$

While κ is not easily measured directly, it can be approximated using measurements from humidified nephelometry. By simultaneously running two nephelometers at different RH, the hygroscopic scattering enhancement factor $f(\mathrm{RH}, \mathrm{RH}_{\mathrm{dry}})$ can be computed, defined as the ratio between the dried and humidified σ_s (Ziemba et al., 2013):

$$f(\mathrm{RH}, \mathrm{RH}_{\mathrm{dry}}) = \frac{\sigma_s(\mathrm{RH})}{\sigma_s(\mathrm{RH}_{\mathrm{dry}})}. \tag{4}$$

Particularly under hygroscopic growth, σ_s and particle volume vary roughly proportionally (Brock et al., 2016), so $f(\mathrm{RH})$ is analogous to g_V when $\mathrm{RH}_{\mathrm{dry}} = 0\ \%$. Consequently, $f(\mathrm{RH}, 0\ \%)$ can be approximated using a variant of Eq. 3, albeit with a distinct κ which we will denote as κ_{sca} (Brock et al., 2016):

$$f(\mathrm{RH}, 0\%) \approx 1 + \kappa_{\mathrm{sca}} \left(\frac{\mathrm{RH}}{1 - \mathrm{RH}} \right). \tag{5}$$

Although $f(\mathrm{RH})$ is usually provided for some $\mathrm{RH}_{\mathrm{dry}} > 0\ \%$, Eq. 4 lets us express the scattering enhancement between any desired $\mathrm{RH}_{\mathrm{wet}}$ and $\mathrm{RH}_{\mathrm{dry}}$ as a function of κ_{sca} and the humidities, which we can then rewrite to isolate κ_{sca}. For the sake of consistency and comparability, $f(\mathrm{RH})$ data are usually provided for standard humidities. For the PACE-PAX dataset in particular, $\mathrm{RH}_{\mathrm{dry}} = 20\ \%$ and $\mathrm{RH}_{\mathrm{wet}} = 80\ \%$, which yields the following expression:

$$\kappa_{\mathrm{sca}} \approx \frac{1 - f(\mathrm{RH})}{f(\mathrm{RH})/4 - 4} \tag{6}$$

As mentioned, this resulting κ_{sca} is distinct from the true, intrinsic κ from Eq. 3. After van Diedenhoven et al. (2022), we assume a linear scaling based on the results presented in Brock et al. (2016), such that

$$\kappa \approx \frac{\kappa_{\mathrm{sca}}}{0.56}. \tag{7}$$

We note that this slope comes with a large uncertainty, which is estimated to be roughly $40\ \%$ (van Diedenhoven et al., 2022).

After applying this correction, the volume water fraction can easily be computed by inserting the resulting value for κ into equations 3 and 2, along with a measurement of the ambient RH.

Hygroscopic scattering enhancement measurements were conducted using a pair of TSI-3563 Scattering Nephelometers aboard the Twin Otter, and prepared and filtered as part of the ISARA algorithm (Schlosser et al., 2025). The data are filtered by a minimum dried and humidified scattering coefficient of $5\ \mathrm{Mm}^{-1}$, and a minimum SPEX airborne AOD_{550} of 0.05, to ensure a sufficient signal to noise ratio.

2.4.2 Effective Radius

We validate the retrievals of the fine-mode effective radius (r_{eff}^{f}) against the ISARA estimate. As the purpose of the ISARA product is to model the effects of humidification on this measurement (among others), the implementation of this comparison is quite straight-forward.

https://doi.org/10.5194/egusphere-2026-6048
Preprint. Discussion started: 17 November 2026
© Author(s) 2026. CC BY 4.0 License.

The ISARA estimate is the effective radius for particles ranging from 0.1 to 1 micron in diameter, humidified to ambient conditions based on a κ-Köhler prescription, similar to what we employ above. It is important to keep in mind that this definition of *fine mode* differs from the one in the SPEX airborne retrieval; it is only a size cutoff, whereas the RemoTAP definition describes spherical particles with a small effective radius, but no strict limit on size. As such, small non-spherical dust particles and large fine-mode particles may respectively "contaminate" the ISARA and RemoTAP estimates.

2.4.3 Number Concentration

We validate the retrievals of N_c against in situ measurements from the DMT Ultra High Sensitivity Aerosol Spectrometer (UHSAS), which is sensitive to particles in the 0.055 to 1 μm diameter range. We exclude measurements within clouds based on the same criteria as above. On the remote sensing side, we limit our analysis to the *fine mode* number concentration specifically, as initial tests were quick to show that, given the retrieved size distributions, only a negligibly small fraction of coarse mode particles –which are far lower in number to begin with– would fall within the size limits of the UHSAS instrument.

The SPEX airborne retrievals do not explicitly contain a vertically resolved number concentration, but one can be constructed from the retrieved aerosol layer height (ALH) and column number; as mentioned, the aerosol layer is represented as a Gaussian, centred around the ALH and with a FWHM of 2 km. However, the ALH retrievals within RemoTAP are associated with large uncertainties, which complicates a direct comparison between the vertical profile described by this Gaussian and the one observed by the Twin Otter. With this in mind, we construct our comparison of the number concentration in such a way that the reliance on the layer height is limited. That is, we compare the average number concentration throughout the densest part of the profile, irrespective of the (measured or retrieved) altitude of the layer. For the SPEX airborne estimate, we define this densest part by the FWHM, i.e., 2 km, which encompasses 76 % of the column by number. An important detail here is that the altitude distributions are truncated at the surface. When the retrieved ALH is sufficiently high, we take the effects of this truncation to be negligible. If the ALH is retrieved to be below 1 km, we might instead use ALH plus 1 km as a modified FWHM. For this dataset, however, this was never the case. As such, we compute the number concentration as $0.76 N_f / 2\mathrm{km}$. For the Twin Otter estimate, we compute the mean number concentration throughout the altitude range containing 76 % of the total measured aerosol load, i.e., between the altitudes corresponding to the 12^{th} and 88^{th} percentiles of the cumulative number distribution.

Finally, following van Diedenhoven et al. (2022), we adjust the SPEX airborne N_c values to accommodate the size range of the in situ measurement by scaling the retrieved number concentration by the fraction of the particles with radii within the size range of the in situ measurement. We use a log-normal particle size number distribution with the effective radius and variance retrieved by RemoTAP, and integrate this distribution between the lower and upper limits of the UHSAS size range. Because the aerosols are dried before the in situ measurement, we compute this correction factor based on the dry size distribution, which we model as the ambient distribution with a modified effective radius $r_{\mathrm{e,dry}}$ defined as

$$r_{\mathrm{e,dry}} = r_{\mathrm{e,wet}}\, g_{\mathrm{V}}^{-1/3}, \tag{8}$$

where the volume growth factor g_{V} is based on the retrieved f_w using Eq. 2.

https://doi.org/10.5194/egusphere-2026-6048
Preprint. Discussion started: 17 November 2026
© Author(s) 2026. CC BY 4.0 License.



2.4.4 SPEX airborne and Twin Otter Collocations

The campaign saw a strong effort toward collocated measurements between the ER-2 and CIRPAS Twin Otter. We focus our analysis on a series of spiral manoeuvres conducted by the Twin Otter, each of which sampled a column of aerosols over a given location which would often be coordinated to be overflown by the ER-2. To produce the vertical profiles we bin the observations to 50 m altitude intervals between the top and bottom of each spiral. We compare the mean across each vertical profile to the mean of all SPEX airborne retrievals within a radius of 20 km of its centre (determined as the mean longitude and latitude throughout the spiral), and within 20 minutes of the moment of closest approach by the ER-2. As a result of the careful coordination between the two aircraft, the time difference between a spiral manoeuvre and a corresponding observation by SPEX airborne is usually within thirty minutes, and at most about an hour. Consecutive upward and downward spirals at the same location are treated as distinct measurements, even when they correspond to a single ER-2 overflight, and consecutive overflights of a single spiral are treated as separate observations if they are more than 30 minutes apart. We only include spirals for which we have at least 10 valid SPEX airborne observations, and for the f_w comparison we further require a minimum of 10 valid measurements of $f(\mathrm{RH})$.

2.5 SPEX airborne versus SPEXone

Whenever possible, ER-2 underflights of the SPEXone swath were conducted. This yielded seven extended ER-2 tracks with collocated PACE observations in (partly) clear-sky conditions, which allow for a direct comparison between the SPEX airborne and SPEXone aerosol retrievals. Throughout these underflights we compare each individual SPEXone pixel to the mean of all corresponding SPEX airborne retrievals within one hour and 2.5 km from its centre, such that the sampled region is similar in size to a SPEXone pixel and utilises the full swath of SPEX airborne.

SPEXone aerosol properties are retrieved using the same version of RemoTAP as is used on SPEX airborne. The data are similarly filtered for χ^2, except we set $\chi^2 < 5$ over land and $\chi^2 < 10$ over ocean, after Fu et al. (2025). In addition, the more sophisticated processing pipeline for SPEXone also allows for more rigorous cloud filtering through a Cloud Fraction (CF) parameter, which is obtained using a neural network-based approach (Yuan et al., 2024; Fu et al., 2025), and which we limit to CF< 0.05. Additionally, to reduce the effects of 3D scattering and spatial stray light, pixels adjacent to a CF> 0.1 pixel are rejected as well. Finally, for ocean retrievals we require that adjacent pixels are also over ocean. These conditions are represented in the retrieval products by the *quality flag* parameter, where a value of 0 denotes a valid retrieval. Where an AOD filter (or similar) is appropriate, we apply this filter to both the SPEXone pixel and the corresponding SPEX airborne average. When comparing a retrieval in the coarse or fine mode separately, we enforce a fine mode AOD fraction (FMF) smaller or greater than 0.5 respectively, and a corresponding fine or coarse mode $\mathrm{AOD}_{550} > 0.05$. For the remaining intrinsic quantities we require a total $\mathrm{AOD}_{550} > 0.1$.

https://doi.org/10.5194/egusphere-2026-6048
Preprint. Discussion started: 17 November 2026
© Author(s) 2026. CC BY 4.0 License.

3 Results and Discussion

3.1 L1C: Radiance and DoLP

In this section we aim to provide a qualitative verification of the polarization and radiance data gathered by SPEXone and SPEX airborne by comparing them to each other, and to the corresponding measurements by RSP. To this end, we focus on the data gathered during the extended ER-2 underflights of the PACE orbit track. For an overview of the instrument specifications for SPEXone, SPEX airborne, and RSP, see Table 1.

For all three polarimeters, L1C data are operationally produced by gridding the geolocated L1B data from all viewing angles onto a rectangular spatial grid, oriented along the flight path. This grid is different for each of the instruments, with SPEXone having the coarsest size at 5.2×5.2 km^2, followed by SPEX airborne with a resolution of 1×1 km^2. For RSP the "grid" is one-dimensional, with an average spacing of 0.18 km. It is noted here that from comparisons of SPEXone with OCI, it has been determined that SPEXone's radiances generated with the current version (V3) of the L0-L1 data processor are systematically biased high by 2.5 %. This has been accounted for in this article by post-processing.

As mentioned, the PACE-PAX campaign produced nine ER-2 flight tracks with opportunities for collocated observations between SPEXone and the ER-2 polarimeters. For one of these tracks (on September 6th), we sample a single location to assess the spectral and angular agreement between the three polarimeters. This track took place over open ocean in clear-sky conditions, and we select a point approximately halfway along the SPEX airborne track, based on the navigational data from the ER-2. For RSP, and in the ALT direction for SPEXone and SPEX airborne, we average the L1C data over a 10 km distance around this target. In the ACT direction we average the full swath for SPEX airborne and only select the nearest grid cells for SPEXone. Given the sun-synchronous orbit of PACE, the overpass in the campaign area is always around 1:00 PM local time. The solar zenith angle was 30° at an azimuth angle of 180°, and the ER-2 heading was 165°. Throughout the overpass, the ground tracks of PACE and the ER-2 were parallel and separated by less than 5 km.

The result can be seen in figure 1. Panels (a) and (c) clearly display the hyper-angular nature of RSP data, whereas (b) and (d) emphasize the hyper-spectral character of SPEXone and SPEX airborne. The large range in DoLP in Fig. 1(a) is the result of Fresnel reflection over water, in combination with the proximity to the principal plane. Taking RSP as the reference, the DoLP measurements by SPEX airborne (nine viewing angles) and SPEXone (five) follow the angular pattern of the RSP data quite well. The radiance data, on the other hand, show large deviations from the RSP measurements for negative viewing zenith angles, with the largest differences near the peak radiance at around -21°. This local maximum results from sunglint, spatially extended by surface winds, which causes large spatial intensity gradients. Because the ground tracks of the ER-2 and PACE are not overlapping, neither do glints as seen from these platforms, resulting in relatively large differences in radiance.

Moving away from the glint, towards positive viewing angles, the agreement between SPEXone and the other polarimeters improves. Panels (b) and (d) respectively show the DoLP and Radiance agreement in the spectral domain for the Nadir viewport. Here we see good agreement across the board, particularly between SPEXone and SPEX airborne. The spectral dependence of the DoLP is almost flat at 0.1, and we see no systematic difference between SPEXone and SPEX airborne, and only a

https://doi.org/10.5194/egusphere-2026-6048
Preprint. Discussion started: 17 November 2026
© Author(s) 2026. CC BY 4.0 License.

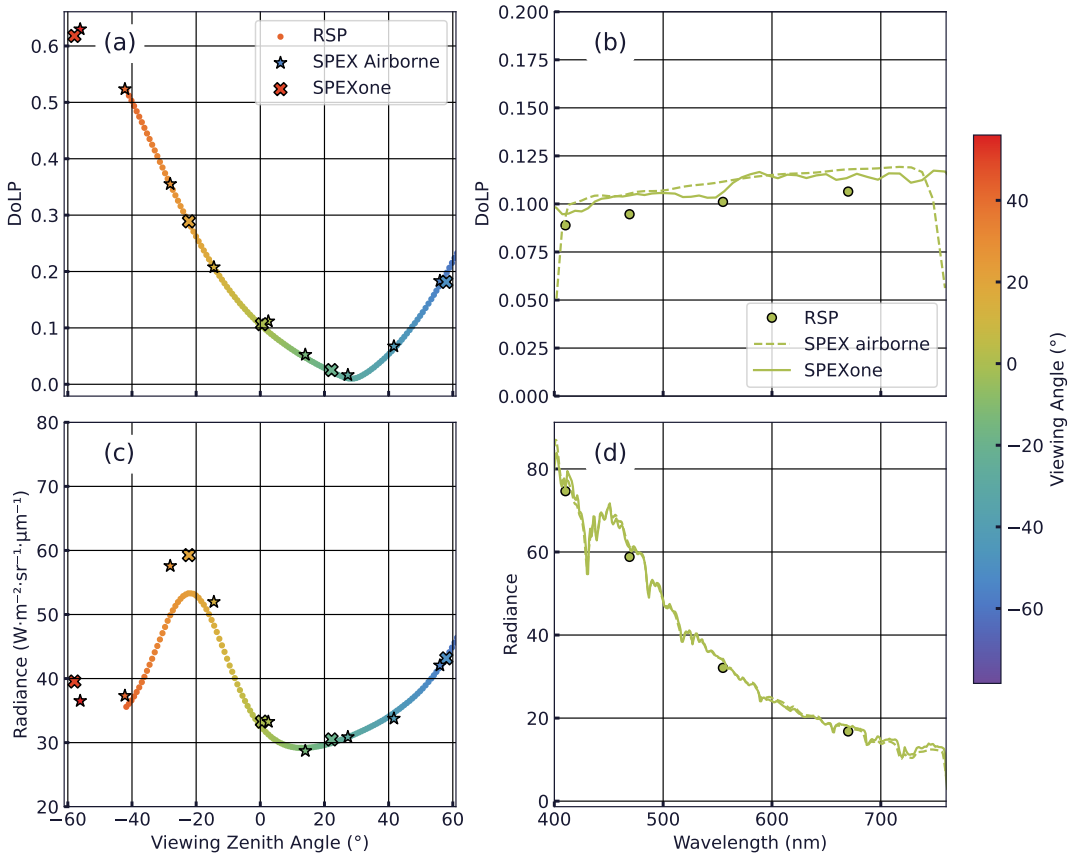


Figure 1. DoLP and Radiance of SPEXone, SPEX airborne and RSP for a clear sky ocean scene on September 06 2024. Plot symbols are indicated in the plot legend. Plot markers are color-coded with their viewing angle value, indicated with the colorbar on the right of the plotregion. Top left (a): DoLP versus viewing zenith angle angle at 555 nm. Viewing zenith angles are taken positive in the northern direction and negative towards the south. Bottom left (c): Radiance versus scattering angle at 555 nm. Rightmost plots: Radiance and DoLP versus wavelength, for nadir viewports. Top right (b): DoLP versus wavelength. Bottom right (d): Radiance versus wavelength.

https://doi.org/10.5194/egusphere-2026-6048
Preprint. Discussion started: 17 November 2026
© Author(s) 2026. CC BY 4.0 License.

small apparent positive bias compared to RSP. In terms of the radiance the agreement between SPEXone and SPEX airborne is particularly convincing, with an rms difference below 3 % in the wavelength range 400-750 nm. Meanwhile the agreement with RSP is once again not quite as impressive, but the measurements are nevertheless consistent with each other.

Next, an intercomparison of all available data over land is provided, both of SPEXone and SPEX airborne versus RSP, and of SPEXone versus SPEX airborne. Before that, an analysis of SPEXone and SPEX airborne versus RSP at a single wavelength is introduced as an intermediate step towards a spectral comparison. This intermediate step provides an indication of the data quality, with a quantitative assessment delivered by the spectral analysis.

We analyse available colocated (PACE+ER-2) clear-sky observations of PACE overpasses over land, where the ER-2 and PACE were heading in the same direction. By limiting the analysis to observations over land, interference from sun-glint is avoided. We compare both SPEXone and SPEX airborne to RSP at a single wavelength of 555 nm. SPEXone and SPEX airborne are collocated to the longitudes and latitudes of individual RSP measurements using bilinear interpolation, and their spectral data are convolved with the RSP response curves. Next, data are averaged from all three instruments to a spatial scale of 5 km, putting the sampling of SPEXone and SPEX airborne on the same footing. For RSP this averaging can only be performed in the ALT direction in the absence of a swath. Viewing zenith angles are then matched by linearly interpolating the RSP data between the closest available angles. We filter data for outliers, by excluding points that deviate by more than five standard deviations. Collocation mismatches of SPEXone and RSP will be larger than for SPEX airborne and RSP due to the fact that the latter two have smaller ground pixels and therefore the averaging scenes are better centered with respect to each other. Assuming collocation differences result in approximately random variations in the difference in DoLP and radiances of collocated RSP and SPEXone observations, we provide mean values per SPEXone viewing angle. The same is done for SPEX airborne to allow for a fair comparison. The result is shown in Fig. 2, where the non-averaged SPEX airborne data are shown as gray dots and the averages of SPEXone and SPEX airborne marked with crosses and stars respectively. Average polarization and radiance data show a good match with RSP for both SPEXone and SPEX airborne, without significant systematic deviations in any data product. The two SPEX instruments show the same level of agreement with RSP; the mean DoLP of SPEXone and SPEX airborne match RSP with differences not larger than 0.003 and 0.005 for SPEXone and SPEX airborne respectively. The averaged radiances of both SPEX instruments agree with RSP's to within 4 %. We conclude that, at this wavelength, both SPEX instruments are in good agreement with RSP, given the uncertainties within both instruments (Table 1).

We further construct a direct comparison between SPEXone and SPEX airborne using all available cloud-free data over land, including also flight-tracks with opposite heading. The procedure is similar to the above comparisons to RSP, except we cannot take advantage of the dense angular sampling of RSP. This means we must rely more heavily on interpolation in the angular domain. Rather than a simple linear scheme, we fit a third order polynomial to the SPEX airborne measurements, which we then resample to the SPEXone viewing zenith angles. Meanwhile the spectral comparison is simplified by the hyperspectral nature of SPEXone and SPEX airborne, so we simply resample the SPEX airborne spectral data to the SPEXone spectral grid using linear interpolation. Figure 3 depicts the result in the form of density plots of the differences between the SPEX airborne and SPEXone DoLP and radiances. We additionally include the median difference and the standard-deviation (solid and dashed

https://doi.org/10.5194/egusphere-2026-6048
Preprint. Discussion started: 17 November 2026
© Author(s) 2026. CC BY 4.0 License.

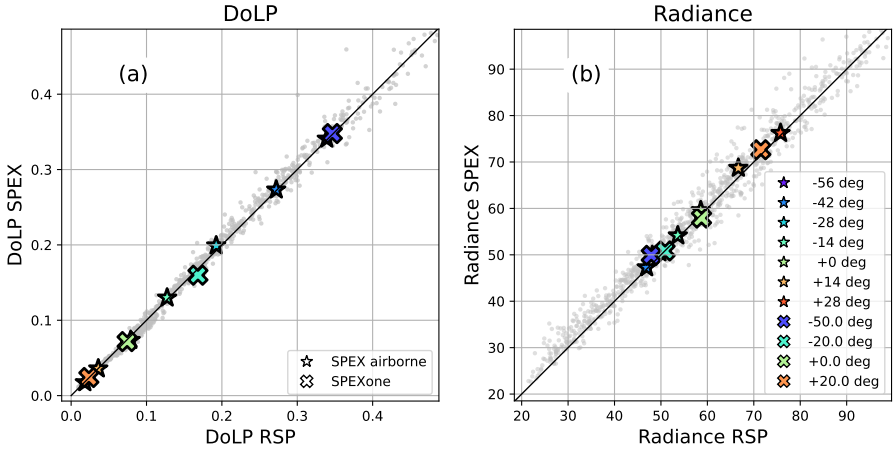


Figure 2. SPEXone and SPEX airborne versus RSP, for two clear sky tracks over land, at 555 nm band of RSP. Panel (a): DoLP of SPEXone and SPEX airborne versus RSP. Panel (b): Radiance of SPEXone and SPEX airborne versus RSP. Radiance is in units Watt/m^2/μm/sr. The solid black line indicates the identity SPEX=RSP. For SPEX-airborne all data (N=1377) are displayed as gray dots, overlaid with the averaged data per viewport of SPEXone and SPEX airborne, where viewing angle indications are given in the legend.

white lines respectively), where, in order to minimize the influence of outliers, we estimate the standard deviation with the inter-quartile range (IQR) and scaling according to a normal distribution. Also shown are the mean differences with RSP for different wavelengths (orange and blue errorbars), based on the same collocation procedure as before.

It can be seen that, in the DoLP, SPEXone compares well to SPEX airborne at wavelengths between 450 nm and 750 nm, with a small negative bias in this wavelength range, which reaches -0.005 near 450 nm. Outside of this wavelength range the (absolute) differences are larger, as low signal levels start to affect the comparison severely. This is similarly visible in the radiances at short wavelengths. Unlike the DoLP, however, the radiances show no clear bias between SPEXone and SPEX airborne.

As for the comparisons to RSP, we find that the conclusions from Fig. 2 can generally be extended to the other wavelengths, with similar agreement but somewhat larger spread in the SPEXone differences due to geolocation mismatches. With the exception of the 410 nm band, we see that the differences with RSP are small, and broadly speaking consistent in magnitude with the differences between SPEXone and SPEX airborne.

We conclude that the SPEXone and SPEX airborne radiance and polarisation data are broadly consistent with each other, as well as with RSP.

https://doi.org/10.5194/egusphere-2026-6048
Preprint. Discussion started: 17 November 2026
© Author(s) 2026. CC BY 4.0 License.

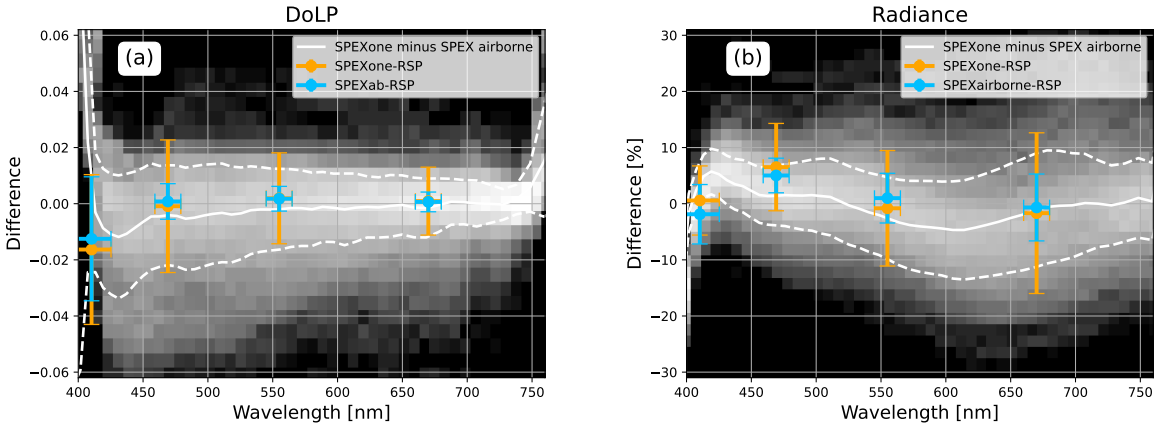


Figure 3. Left: Difference in DoLP, SPEXone minus SPEX airborne, versus wavelength. Right: Difference in radiance, SPEXone minus SPEX airborne in %, versus wavelength, for all five viewing angles together in a density plot. The white line is the average difference and the dashed line the standard deviation. Also shown are the differences between the SPEX instruments and RSP for each applicable wavelength band within the RSP data. The points (orange for SPEXone, blue for SPEX airborne) show the median difference with RSP, with vertical bars representing the standard-deviation computed using the same IQR estimator as above and horizontal bars showing the width of the RSP wavelength bands.

3.2 SPEX airborne versus AERONET

We quantify the agreement between SPEX airborne and AERONET using the Root Mean Square Deviation (RMSD) between the measurements, in addition to the bias (the difference between the marginal means). Finally, we use the percentage of collocations where the error is within the range proposed by the Global Climate Observing System (GCOS), modified slightly to accommodate the uncertainties in the AERONET measurements (Popp et al., 2016). For the AOD, this requirement amounts to an absolute error of 0.04, or a relative error of 10 %, whichever is larger, and for the SSA the absolute error should be smaller than 0.03. GCOS does not formulate a requirement for AE, but we require an absolute error smaller than 0.2, as used in Hasekamp et al. (2024). These are the same metrics that were previously used to evaluate the performance of SPEXone in Fu et al. (2025), which allows us to easily compare the performance of the two instruments. We do note, however, that the SPEXone study is more extensive in both space and time, making use of the global AERONET network and six months worth of satellite data, as opposed to a single month within a small region.

The collocations between SPEX airborne and AERONET are shown in Fig. 4, and the corresponding metrics are summarised in table 2. We only compute these metrics for the retrievals over land, as there are not enough collocations over ocean to justify a statistical interpretation, but we nevertheless note that we do not see large differences in performance between these two surface types.

The AOD performance of SPEX airborne is similar to that of SPEXone, with a slightly smaller RMSD and bias (0.045 and -0.004 versus 0.053 and -0.017), and a similar adherence to the GCOS requirement. This remains true when filtering for

https://doi.org/10.5194/egusphere-2026-6048
Preprint. Discussion started: 17 November 2026
© Author(s) 2026. CC BY 4.0 License.

low-AOD cases only ($AOD_{532} < 0.2$), although SPEX airborne sees a smaller improvement than SPEXone. This is consistent with the generally low AOD throughout PACE-PAX, as low-AOD cases are over-represented in the dataset.

In the AE the performance of SPEX airborne is again in line with SPEXone's. Because of the low aerosol loads we opt for a more lenient lower limit on the AOD than Fu et al. (0.1 rather than 0.2), which comes at the cost of retrieval reliability, but nevertheless we see that the results for SPEX airborne only fall slightly short of SPEXone in terms of RMSD (0.315 versus 0.251), while the two other metrics are approximately identical.

In the SSA comparison we see that SPEX airborne seems to overestimate high-SSA cases and overestimate low-SSA cases relative to AERONET. While SPEXone shows a similar tendency, SPEX airborne's overall agreement with AERONET falls short of SPEXone's across all three metrics. Once again, we attribute this difference in performance to the low AOD throughout the campaign. The AERONET retrievals of the SSA are particularly reliant on high AOD, requiring a minimum AOD_{440} of 0.4 for quality assurance (Dubovik et al., 2000; Holben et al., 2006; Sinyuk et al., 2020), which is rarely reached in this particular sample. As such, the AERONET retrievals likely contain sizeable errors themselves, and should not be interpreted as the ground truth. Even when the minimum AOD is disregarded entirely, however (not shown), the difference in performance between SPEX airborne and SPEXone remains, so errors in the AERONET retrievals may not be solely responsible. In Sect. 3.4 we directly compare the retrievals from SPEX airborne and SPEXone, which provides some further insight into this matter.

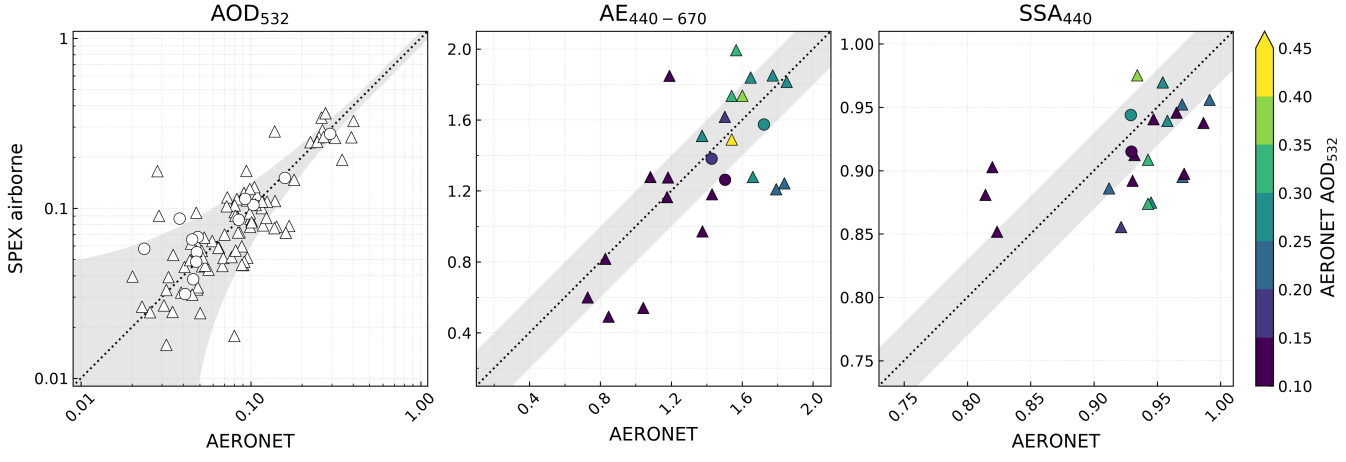


Figure 4. Comparisons between SPEX airborne and AERONET measurements of the AOD, AE, and SSA for collocations over land (triangles) and over ocean (circles). The shaded areas show the modified GCOS requirements. The colors in the AE and SSA panels show the AERONET AOD.

3.3 SPEX airborne versus Twin Otter In Situ

The comparisons between the SPEX airborne retrievals and the airborne in situ measurements from aboard the CIRPAS Twin Otter are shown in Fig. 5, and additionally provided as a table in App. A.

https://doi.org/10.5194/egusphere-2026-6048
Preprint. Discussion started: 17 November 2026
© Author(s) 2026. CC BY 4.0 License.

Table 2. Performance of SPEX airborne against AERONET. This table only shows the results for retrievals over land, as there are not nearly enough comparisons over ocean to justify any statistical analysis.

Retrieval	Num	RMSD	Bias	REQ
AOD_{532}	91	0.045	−0.004	74.7 %
AOD_{532} ($AOD_{532} < 0.2$)	79	0.038	−0.004	79.8 %
$AE_{440\text{-}670}$ ($AOD_{532} > 0.1$)	23	0.315	−0.042	60.9 %
SSA_{440} ($AOD_{532} > 0.1$)	21	0.048	−0.018	42.9 %

Beginning with the volume water fraction f_w, we see that the in situ and remote sensing estimates are in approximate agreement, with all points falling within the range associated with the estimated error on n_{dry} (± 0.04). As expected given the arid climate in the region, the observed water fractions are very low (< 0.2) over land, and notably elevated over ocean. In addition to an elevated RH, these ocean overpasses also saw an increase in hygroscopicity (table A1), consistent with a greater contribution from marine aerosols. Note that two spirals cannot be made out in the figure because they overlap two others. These points correspond to pairs of spirals (ascending+descending) at the same location. By treating these as separate observations we can get a sense of the temporal variability of the aerosol conditions, which in this case is clearly limited. From this we conclude that the time difference between the Twin Otter and ER-2 observations is unlikely to be an important contributor of errors. Given the systematic uncertainty in our estimation of κ, as well as the aforementioned uncertainty in n_{dry}, the measurements are in good agreement. Overall, these results are consistent with the results presented in van Diedenhoven et al. (2022), wherein a similar validation of the RSP-retrieved water fraction was conducted. This further increases confidence in this polarimeter retrieval of the water fraction.

The r_{eff}^{f} comparison shows good agreement overall. SPEX airborne appears to be biased slightly low relative to the in situ estimate, which is mostly driven by the observations on 0913. The spirals with the highest f_w (that is, those on 0926) correspond to the largest effective radius as well. Here, the agreement between RemoTAP and ISARA further indicates that the water uptake is represented consistently between the remote and in situ estimates.

The N_c^f comparison, much like that of f_w, contains a visible separation between spirals over land and over ocean, with N_c^f highest over land and lowest over ocean. The in situ and remote estimates are well correlated, but the SPEX airborne retrieval is biased high by a factor of 2 or more with respect to the Twin Otter observations. One contributing factor to this bias may be the presence of aerosols at altitudes below or above the range sampled by the Twin Otter, which would naturally result in an apparent overestimation by SPEX airborne. Dust and sea spray aerosols tend to be most concentrated near the surface, and the wildfire activity in the area may have produced layers of biomass burning aerosols at higher altitudes. While we expect this to be an important factor in some cases, however, we deem it unlikely that every observation in the sample should be so strongly affected in this way. Furthermore, the number concentration is based on the underlying assumption of a single Gaussian layer

https://doi.org/10.5194/egusphere-2026-6048
Preprint. Discussion started: 17 November 2026
© Author(s) 2026. CC BY 4.0 License.

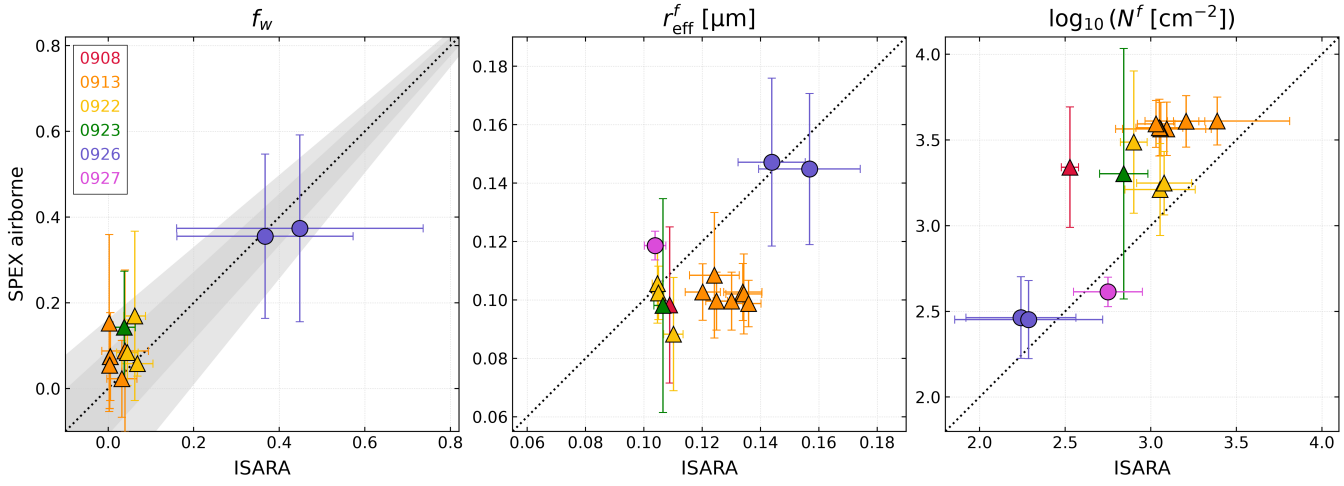


Figure 5. SPEX airborne retrievals of f_w, r_{eff}^f, and N_c^f compared to the corresponding in situ measurements during Twin Otter spiral manoeuvres, with the standard deviations shown as the error ranges. Circles and triangles denote observations over ocean and land respectively, and points are coloured by date. In the f_w panel the shaded regions correspond to the uncertainty ranges (± 0.02 and ± 0.04) in the refractive index of dry material.

with a FWHM of 2 km, which may be inaccurate. To produce the observed positive bias, however, the true width of the aerosol layer would need to be on the order of 4 km, which is rather unlikely.

Beyond these methodological considerations, the discrepancy could also be explained as a bias within the SPEX airborne retrievals of N^f. While the RemoTAP algorithm uses the column number in its derivation of the AOD (and we find that the AOD retrievals are of high quality), a bias in the column number can be offset by an opposite bias in the effective radius, leaving the AOD retrieval unaffected. Though we do see a slight negative bias in the effective radius comparison, it is not large enough produce the bias in the number concentration by itself. We further illustrate this in Appendix B, where we apply a "correction" to the SPEX airborne estimate based on the ISARA effective radius, which does improve the agreement, but does not entirely eliminate the bias.

A similar comparison between polarimeter (RSP) and in situ number concentrations was presented in van Diedenhoven et al. (2022). That study did not see a similar bias, though their observations exclusively took place over ocean (where we do not see a bias either) and the study was conducted with a different instrument and retrieval algorithm. In the absence of a more direct point of comparison, then, we may conclude that the SPEX airborne-RemoTAP retrieval of the number concentration is biased high over land.

3.4 SPEX airborne versus SPEXone

Because the same version of the RemoTAP algorithm is used for the aerosol retrievals on SPEXone and SPEX airborne, both instruments retrieve the same aerosol parameters. This makes it relatively easy to compare the full suite of aerosol properties

https://doi.org/10.5194/egusphere-2026-6048
Preprint. Discussion started: 17 November 2026
© Author(s) 2026. CC BY 4.0 License.

between these two instruments. For the sake of brevity, we focus on the properties used in the above comparisons to AERONET and the Twin Otter, namely the AOD, AE, SSA, f_w, r_{eff}^f, and N^f.

The result can be seen in Fig. 6. We see that the agreement in the AOD is quite good, and consistent with the AERONET validations, with the notable exception of a number of correlated outliers (highlighted in red). These collocations all took place on September 30$^{\text{th}}$, over a small patch of open ocean with high surface wind speeds. We attribute the discrepancy to sun-glint, which at high wind speeds is known to occasionally be interpreted by RemoTAP as an excess of strongly absorbing fine mode aerosol. The resulting disagreement between SPEX airborne and SPEXone is then easily explained by the difference in solar zenith angle (with the ER-2 and PACE overflights being an hour apart) and viewing geometry. This issue has since been addressed in a version upgrade to the RemoTAP algorithm (Fu et al., 2026), and indeed, internal tests with this new version have found much better agreement for this case. Given this identified retrieval issue, we exclude these collocations on this track from further analysis. It bears mentioning that the identification and diagnosis of this issue was greatly expedited by the availability of corroborating PACE-PAX airborne measurements, which underscores the importance of this type of validation campaign.

Overall, the AODs are even lower than in the AERONET comparison (Fig. 4, and we see that the polarimeters remain in good agreement. As a consequence of the low AODs, however, the validations of the remaining aerosol retrievals (all of which perform best at high AOD) are limited by the number of suitable observations.

After filtering for $\text{AOD}_{550} > 0.1$, we are left with 37 collocations, with approximately half (17) taking place on 0906, another half (20) on 0927. All but 7 of these observations took place over ocean. Thus, for the statistical interpretation of these results it is important to keep in mind that the range of aerosol and surface conditions included in this sample is limited, and the data are not independent. To somewhat alleviate this constraint, we additionally show the collocations where the AOD is slightly below the threshold value, but within 0.025. While officially rejected, these points can provide some insight into the dependence on the AOD, and increase the number of collocations over land.

We see that the agreement in the AE is mostly in line with the results presented in Fu et al. (2025). The observed values are somewhat low by comparison, however, with the majority of observed AE between 0.8 and 1.4. This suggests that the observed aerosols are more coarse than the global average, which may be expected given the arid climate. Interestingly, however, the range of values in our own comparison to AERONET (Fig. 4) more closely resembles the global distribution, and seem mostly unaffected by such effects. Nevertheless, we find that the performance of SPEXone and SPEX airborne is maintained throughout this lower range of AE.

In the SSA, we see that SPEX airborne shows better agreement with SPEXone than with AERONET, with a smaller RMSD and bias. The observed SSA in this sample are lower than those in the AERONET comparisons (Fig. 4 and Fu et al. (2025)). This could be attributed to biomass burning activity in the region. Given the small number of AERONET observations of the SSA, the qualitative difference from the distribution in Fig. 4 may then simply be explained by sampling effects. Whatever the cause may be, however, we see that the agreement in the SSA remains consistent for these lower values.

Relative to SPEX airborne, SPEXone has a tendency to underestimate low SSA, and overestimate high SSA. This is consistent with our findings in Sect. 3.2: both SPEXone and SPEX airborne appear to exhibit this same behaviour relative to

https://doi.org/10.5194/egusphere-2026-6048
Preprint. Discussion started: 17 November 2026
© Author(s) 2026. CC BY 4.0 License.

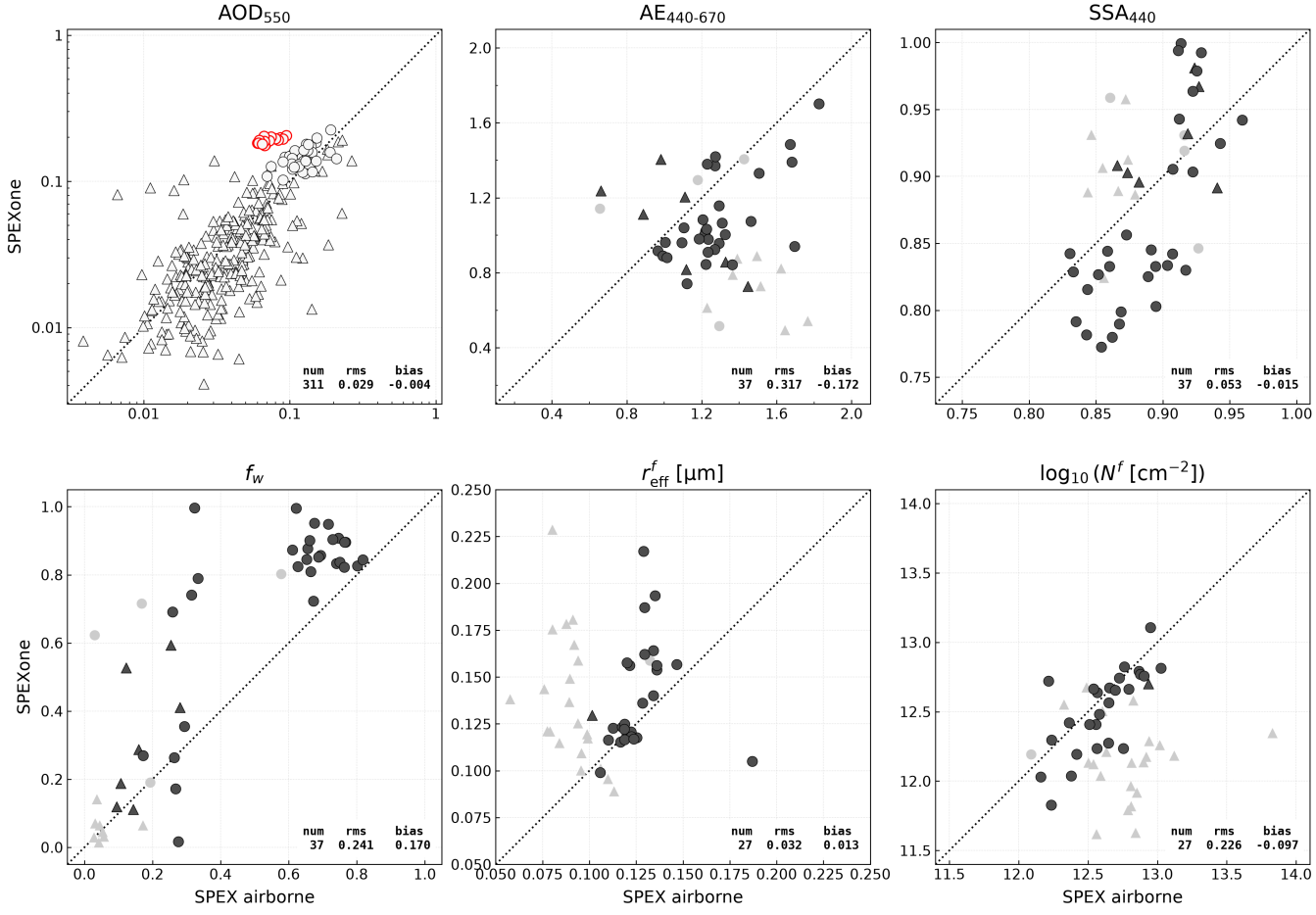


Figure 6. Comparisons between SPEX airborne and SPEXone retrievals during the ER-2 underflights of the PACE track. The top row shows the parameters which were previously validated against AERONET, i.e., from left to right: AOD, AE, and SSA, and the parameters in the bottom row are those used in the comparison to in situ measurements, i.e., f_w, r_{eff}^f, and N^f. As before, circles are observations over ocean and triangles are observations over land. The dark points are collocations with sufficient AOD, and the lighter points are those where the AOD falls slightly short (i.e., within 0.025 of the minimum). In the AOD panel all collocations on 20240930 are marked in red.

AERONET, but the effect is stronger for SPEX airborne. Although the conclusions from Sect. 3.2 only apply to collocations over land, the qualitative similarity is notable.

We now move on to the parameters used in the validation against the in situ measurements, namely f_w, r_{eff}^f and N_c^f, where the latter is predominantly composed of N^f (the ALH also plays a minor role; its performance is evaluated in the supplement). The comparison of f_w shows good agreement for dry aerosol, and a bias of around 0.2 at high (> 0.5) water fractions. For moderate f_w the agreement is not quite as strong, with SPEXone seemingly biased high relative to SPEX airborne.

https://doi.org/10.5194/egusphere-2026-6048
Preprint. Discussion started: 17 November 2026
© Author(s) 2026. CC BY 4.0 License.

The agreement in the effective radius is satisfactory over ocean, especially at low r_{eff}. Over land (and at low AOD), SPEXone appears to be biased high relative to SPEX airborne. Given our findings in sect. 3.3, it may be more appropriate to interpret this as an underestimation by SPEX airborne.

Finally, the fine-mode column number comparison shows good agreement as long as the FMAOD is sufficiently high. For lower FMAOD (and particularly over land) SPEX airborne overestimates compared to SPEXone by up to an order of magnitude. Much like our findings in Sect. 3.3, this disagreement is quantitatively consistent with the opposite bias in the effective radius. The presence of these biases relative to both the in situ measurement and SPEXone suggests that SPEXone may be more consistent with these in situ measurements than SPEX airborne, at least over land, and at low AOD. We do note, however, that applying a modest FMAOD filter did not appreciably affect the results in Sect. 3.3.

Additional comparisons for the remaining RemoTAP aerosol retrievals are provided as a supplement. Overall, we find that the agreement between SPEX airborne and SPEXone is satisfactory, indicating that SPEX airborne is a good proxy for SPEXone.

4 Conclusions

We present our efforts toward validating the aerosol retrievals from SPEXone on PACE using data gathered during the PACE-PAX campaign.

As a start, we compare the level 1C (radiance and DoLP) measurements of SPEXone and SPEX airborne to those from the reference polarimeter RSP, making use of the collocated observations between PACE and the ER-2. Comparing the radiance and DoLP for each viewing angle throughout all clear-sky collocations over land, we find excellent agreement between SPEX airborne and RSP. Differences between SPEXone and RSP are slightly larger, which we attribute to a more challenging collocation. We then extend our analysis with a direct comparison between SPEX airborne and SPEXone at L1C, where we interpolate the SPEX airborne measurements to SPEXone's viewing angles. These results show some contamination by instrument noise at the highest and lowest wavelengths, and a slight negative bias (no more than -0.005) in the SPEXone DoLP compared to SPEX airborne. Overall, the mean differences between SPEXone, SPEX airborne, and RSP are within the instruments' accuracies.

To validate the aerosol products, we begin by validating the SPEX airborne retrievals of the AOD, AE, and SSA against AERONET, drawing on previous work by Fu et al. to gauge the similarity to SPEXone. We find that in terms of the AOD and AE SPEX airborne performs very well, and is in line with SPEXone. In the SSA, meanwhile, the agreement lags behind slightly; SPEX airborne appears to overestimate low SSA and underestimate high SSA. We may attribute this for the most part to a lack of high-AOD collocations during the campaign, as both the SPEX airborne and in particular the AERONET retrievals are reliant on high AOD.

We additionally validate the retrievals of the volume water fraction f_w, and the fine mode effective radius r_{eff}^f and number concentration N_c^f through a comparison to in situ measurements taken aboard the CIRPAS Twin Otter aircraft. We compile vertical profiles from spiral manoeuvres conducted by the Twin Otter, and compare their averages to the corresponding collocated SPEX airborne observations. We find convincing agreement in the f_w comparison, with all points falling within the

https://doi.org/10.5194/egusphere-2026-6048
Preprint. Discussion started: 17 November 2026
© Author(s) 2026. CC BY 4.0 License.

predicted range given the uncertainty in the assumed dry refractive index. Although the majority of the observed aerosols were particularly dry ($f_w < 0.2$). Taken together with previous work (e.g., van Diedenhoven et al. (2022)), this work further demonstrates the water fraction retrievals for different combinations of aerosol, surface, and meteorology. As the uptake of ambient water by aerosols plays an important role in both aerosol-radiation and aerosol-cloud interactions, this satellite retrieval of the water fraction can be of great value in constraining the aerosol radiative forcing.

We find good agreement in r_{eff}^f, with a small negative bias in SPEX airborne relative to the ISARA estimate which is mostly driven by observations on a single day. The agreement at elevated f_w is particularly notable here, as it suggests a successful conversion to ambient conditions by the ISARA algorithm.

We find that the N_c^f retrieved by SPEX airborne tends to be biased high by $200 - 300$ % over land. We posit that this bias may in part be explained by a combination of aerosols at high altitudes or near the surface (where they could not be sampled by the Twin Otter), and the aforementioned slight underestimation of the effective radius. Over ocean the agreement is somewhat better, and consistent with previous work on the CAMP^{2}EX and ACTIVATE campaigns (van Diedenhoven et al., 2022), albeit with a small sample. To our knowledge, other similar validations of polarimeter retrievals of the column number or number concentration have not been conducted to date, but we suggest that future work might make use of the LIDAR profiles which are also available for this dataset to produce a vertically-resolved number concentration product, c.f. Schlosser et al. (2022).

Finally, we directly compare the SPEX airborne and SPEXone aerosol retrievals throughout the series of extended underflights of the PACE orbit track by the ER-2. Beginning with the properties previously used in the AERONET validation, we find good agreement in the AOD, with the exception of a number of correlated outliers where SPEXone appears to significantly overestimate compared to SPEX airborne. We attribute this disagreement to a retrieval issue related to sun-glint at high wind speeds. This issue has since been addressed in an update of the RemoTAP algorithm (Fu et al., 2026).

In terms of the SSA, the SPEX instruments seem to be in better agreement with each other than with AERONET. This is likely the result of a more precise collocation, as well as the higher tolerance for low AOD afforded by the design of the polarimeters. In the AE the agreement is in line with the results presented in Fu et al. (2025), though SPEXone appears to be biased slightly low relative to SPEX airborne over ocean. In all three cases (AOD, AE, and SSA), these direct comparisons between SPEX airborne and SPEXone complement the validations against AERONET by covering lower values.

Next, comparing the f_w, r_{eff}^f, and N^f, we see satisfactory agreement for the most part. The f_w comparison shows that the instruments agree on both the low and high water content extremes, with an overestimation by SPEXone in the middling regime. The agreement in the effective radius is satisfactory, and best at low values. When AOD is low over land, SPEXone is biased high relative to SPEX airborne. Finally, the N^f comparison shows good agreement, as long as the FMAOD is sufficiently high. For lower AOD the result is an apparent underestimation by SPEXone, though a positive bias in SPEX airborne may be a more appropriate interpretation given the aforementioned comparisons to the in situ measurements, as well as the comparisons of the effective radius.

Overall, we find that SPEXone and SPEX airborne perform similarly well across a range of metrics, and we conclude that SPEX airborne is a good proxy for SPEXone.

https://doi.org/10.5194/egusphere-2026-6048
Preprint. Discussion started: 17 November 2026
© Author(s) 2026. CC BY 4.0 License.

Appendix A: Table of SPEX airborne and Twin Otter spiral collocations

Table A1. Overview of the collocations between SPEX airborne and spiral manoeuvres by the CIRPAS Twin Otter, corresponding to the points in figure 5. The "Time" column shows the UTC time at the approximate midpoint of the spiral manoeuvre. Data are shown as the mean and standard-deviations, and dashes represent missing data due to one (or more) of the filtering requirements outlined in the main body.

	Surface	Date	Time	$\log_{10}(N_c^f\ [\mathrm{cm}^{-3}])$		r_{eff}^f		f_w		κ	RH [%]
				SPEX	Twin Otter	SPEX	Twin Otter	SPEX	Twin Otter		
S1	Land	0908	21:38	3.34 ± 0.35	2.53 ± 0.05	0.10 ± 0.03	0.11 ± 0.00	0.44 ± 0.17	–	0.04 ± 0.04	31 ± 6
S2	Land	0913	17:44	3.61 ± 0.15	3.21 ± 0.11	0.10 ± 0.01	0.13 ± 0.01	0.07 ± 0.10	0.00 ± 0.00	0.02 ± 0.02	18 ± 7
S3	Land	0913	17:57	3.61 ± 0.15	3.21 ± 0.07	0.10 ± 0.01	0.12 ± 0.00	0.07 ± 0.10	0.01 ± 0.00	0.02 ± 0.02	19 ± 8
S4	Land	0913	18:18	3.56 ± 0.16	3.09 ± 0.26	0.10 ± 0.01	0.13 ± 0.01	0.05 ± 0.10	0.00 ± 0.00	0.01 ± 0.01	16 ± 6
S5	Land	0913	18:34	3.56 ± 0.16	3.06 ± 0.26	0.10 ± 0.01	0.12 ± 0.01	0.05 ± 0.10	0.00 ± 0.00	0.02 ± 0.01	15 ± 6
S6	Land	0913	18:53	3.61 ± 0.14	3.39 ± 0.42	0.11 ± 0.02	0.12 ± 0.01	0.15 ± 0.21	0.00 ± 0.00	0.02 ± 0.04	17 ± 5
S7	Land	0913	21:15	3.57 ± 0.17	3.05 ± 0.14	0.10 ± 0.01	0.13 ± 0.01	0.09 ± 0.19	0.04 ± 0.05	0.09 ± 0.04	23 ± 18
S8	Land	0913	21:38	3.59 ± 0.14	3.03 ± 0.11	0.10 ± 0.01	0.14 ± 0.00	0.02 ± 0.09	0.03 ± 0.04	0.09 ± 0.02	22 ± 16
S9	Land	0922	18:19	3.49 ± 0.42	2.90 ± 0.08	0.09 ± 0.02	0.11 ± 0.00	0.17 ± 0.20	0.06 ± 0.03	0.12 ± 0.05	36 ± 8
S10	Land	0922	19:23	3.21 ± 0.27	3.05 ± 0.21	0.11 ± 0.01	0.10 ± 0.00	0.08 ± 0.08	0.04 ± 0.03	0.09 ± 0.05	32 ± 9
S11	Land	0922	19:53	3.25 ± 0.19	3.08 ± 0.16	0.10 ± 0.01	0.10 ± 0.00	0.06 ± 0.03	0.07 ± 0.04	0.14 ± 0.07	33 ± 8
S12	Land	0923	19:33	3.30 ± 0.73	2.84 ± 0.14	0.10 ± 0.04	0.11 ± 0.00	0.14 ± 0.13	0.04 ± 0.03	0.09 ± 0.05	27 ± 8
S13	Ocean	0926	19:38	2.46 ± 0.24	2.24 ± 0.32	0.14 ± 0.03	0.16 ± 0.02	0.37 ± 0.22	0.45 ± 0.29	0.21 ± 0.09	23 ± 31
S14	Ocean	0926	20:42	2.45 ± 0.23	2.29 ± 0.43	0.15 ± 0.03	0.14 ± 0.01	0.36 ± 0.19	0.37 ± 0.21	0.23 ± 0.07	19 ± 27
S15	Ocean	0927	23:00	2.61 ± 0.09	2.75 ± 0.20	0.12 ± 0.00	0.10 ± 0.00	–	0.02 ± 0.02	0.09 ± 0.07	10 ± 6

https://doi.org/10.5194/egusphere-2026-6048
Preprint. Discussion started: 17 November 2026
© Author(s) 2026. CC BY 4.0 License.

Appendix B: Comparison to the ISARA number concentration when accounting for biases in the effective radius

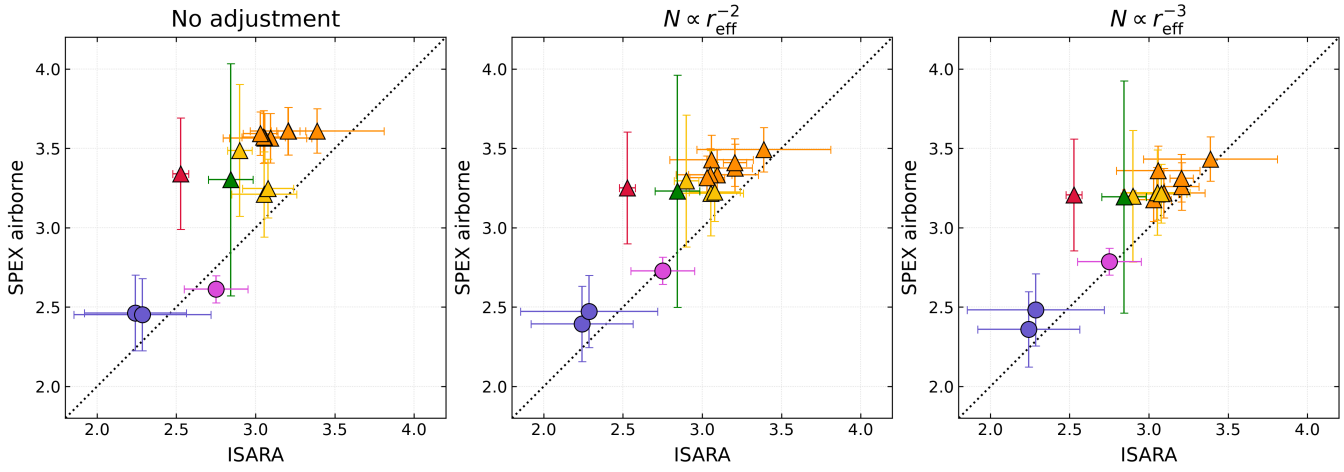


Figure B1. Alternate versions of the N_c^f comparison from the main body, where the SPEX airborne data are corrected by assuming ISARA r_{eff}^f to be the ground truth. From left to right: the standard processing pipeline (Fig. 5); adjusted assuming Mie scattering; adjusted assuming Rayleigh scattering. As a result of the corrections, both the spread and the bias of the data decrease. Nevertheless, a bias remains.

As outlined in the main body, the SPEX airborne number concentration estimate is biased high relative to the in situ estimate, while the effective radius is biased slightly low. We investigate if this bias in the former can simply be explained by the bias in the latter, by applying a correction to the SPEX airborne number concentration. Assuming that the SPEX airborne AOD is (approximately) correct, and should thus be held constant, and neglecting variations in the scattering efficiency factor, the column number approximately scales with r_{eff}^{-2}. We can then compute a "corrected" column number, which accounts for the difference in effective radius, as follows:

$$N' = \left(\frac{r_{\text{eff,spex}}}{r_{\text{eff,isara}}} \right)^2 N. \tag{B1}$$

In the Rayleigh regime, the extinction scales with volume, rather than area. Thus, for the finest particles, we might replace this square with a cube. In this case, given the range of particle sizes, we might expect the appropriate exponent to fall somewhere between 2 and 3.

The result of applying such a correction can be seen in Fig. B1. The corrections appear to improve the comparisons both in terms of bias and spread, but, while the bias is mitigated, it is not eliminated entirely. We conclude that the observed overestimation of the number concentration is partially, but not entirely, explained by an opposite bias in the effective radius, and vice-versa.

https://doi.org/10.5194/egusphere-2026-6048
Preprint. Discussion started: 17 November 2026
© Author(s) 2026. CC BY 4.0 License.

Data availability. The PACE-PAX campaign data used in this study are publicly available to download from the NASA Earthdata servers. These include the ISARA dataset of in situ measurements from aboard the Twin Otter (Revision 3 used here), as well as the SPEX airborne and RSP datasets (Knobelspiesse et al., 2025a). SPEXone data are also publicly available on NASA servers (NASA Ocean Biology Processing Group, 2025a, b, c).

Author contributions. The data analysis for the comparisons at L1C was conducted by BS and MS. Processing of the SPEX airborne data was done by GF and OH. The text was written by JM and MS, and edited by BvD. The sections pertaining to the L1C data acquisition and comparisons to RSP were written by MS, and the remainder was written by JM. BC and JS respectively provided the RSP and ISARA data used in the comparisons, and provided feedback on the manuscript.

Competing interests. One of the authors is a member of the editorial board of Atmospheric Measurement Techniques. The authors have no further competing interests to declare.

Acknowledgements. JM acknowledges support from the Dutch Research Council (NWO) and the Netherlands Space Office (NSO), through grant no. ENW.GO.002.004 (https://doi.org/10.61686/ZXNQB69586).

This research would not have been possible without the contributions from the entire PACE-PAX team. We especially thank Kirk Knobelspiesse and Ivona Cetinić, who, alongside Brian Cairns, were instrumental in the organisation of the campaign, and Luke Ziemba, who lead the in situ data collection by the CIRPAS Twin Otter. Finally, the authors express their gratitude for the public availability of the AERONET data.

https://doi.org/10.5194/egusphere-2026-6048
Preprint. Discussion started: 17 November 2026
© Author(s) 2026. CC BY 4.0 License.

References

Amerongen, A. v., Rietjens, J., Campo, J., Dogan, E., Dingjan, J., Nalla, R., Caron, J., and Hasekamp, O.: SPEXone: a compact multi-angle polarimeter, in: International Conference on Space Optics — ICSO 2018, vol. 11180, pp. 223–236, SPIE, https://doi.org/10.1117/12.2535940, 2019.

Brock, C. A., Wagner, N. L., Anderson, B. E., Attwood, A. R., Beyersdorf, A., Campuzano-Jost, P., Carlton, A. G., Day, D. A., Diskin, G. S., Gordon, T. D., Jimenez, J. L., Lack, D. A., Liao, J., Markovic, M. Z., Middlebrook, A. M., Ng, N. L., Perring, A. E., Richardson, M. S., Schwarz, J. P., Washenfelder, R. A., Welti, A., Xu, L., Ziemba, L. D., and Murphy, D. M.: Aerosol optical properties in the southeastern United States in summer – Part 1: Hygroscopic growth, Atmospheric Chemistry and Physics, 16, 4987–5007, https://doi.org/10.5194/acp-16-4987-2016, 2016.

Cairns, B., Russell, E. E., and Travis, L. D.: Research Scanning Polarimeter: calibration and ground-based measurements, in: Polarization: Measurement, Analysis, and Remote Sensing II, vol. 3754, pp. 186–196, SPIE, https://doi.org/10.1117/12.366329, 1999.

Campo, J., Rietjens, J. H. H., Arko, M., Smit, M., Siemons, M., Laasner, R., Eigenraam, A., Tol, P., Vretenar, M., Winkelman, R., Nalla, R. K., Dingjan, J., Borst, G., Oort, M., van Hees, R. M., van Diedenhoven, B., Landgraf, J., and Hasekamp, O.: Design, calibration and unique resulting science of SPEXone on PACE and its second generation successor, in: Sensors, Systems, and Next-Generation Satellites XXIX, edited by Babu, S. R., Hélière, A., and Urabe, T., vol. 13667, p. 136670E, International Society for Optics and Photonics, SPIE, https://doi.org/10.1117/12.3072068, 2025.

Daimon, M. and Masumura, A.: Measurement of the refractive index of distilled water from the near-infrared region to the ultraviolet region, Applied Optics, 46, 3811–3820, https://doi.org/10.1364/AO.46.003811, 2007.

Diner, D. J., Xu, F., Garay, M. J., Martonchik, J. V., Rheingans, B. E., Geier, S., Davis, A., Hancock, B. R., Jovanovic, V. M., Bull, M. A., Capraro, K., Chipman, R. A., and McClain, S. C.: The Airborne Multiangle SpectroPolarimetric Imager (AirMSPI): a new tool for aerosol and cloud remote sensing, Atmospheric Measurement Techniques, 6, 2007–2025, https://doi.org/10.5194/amt-6-2007-2013, 2013.

Dubovik, O., Smirnov, A., Holben, B. N., King, M. D., Kaufman, Y. J., Eck, T. F., and Slutsker, I.: Accuracy assessments of aerosol optical properties retrieved from Aerosol Robotic Network (AERONET) Sun and sky radiance measurements, Journal of Geophysical Research: Atmospheres, 105, 9791–9806, https://doi.org/10.1029/2000JD900040, 2000.

Fan, C., Fu, G., Noia, A. D., Smit, M., Rietjens, J. H. H., Ferrare, R. A., Burton, S., Li, Z., Hasekamp, O. P., Fan, C., Fu, G., Noia, A. D., Smit, M., Rietjens, J. H. H., Ferrare, R. A., Burton, S., Li, Z., and Hasekamp, O. P.: Use of A Neural Network-Based Ocean Body Radiative Transfer Model for Aerosol Retrievals from Multi-Angle Polarimetric Measurements, Remote Sensing, 11, https://doi.org/10.3390/rs11232877, company: Multidisciplinary Digital Publishing Institute Distributor: Multidisciplinary Digital Publishing Institute Institution: Multidisciplinary Digital Publishing Institute Label: Multidisciplinary Digital Publishing Institute, 2019.

Fu, G. and Hasekamp, O.: Retrieval of aerosol microphysical and optical properties over land using a multimode approach, Atmospheric Measurement Techniques, 11, 6627–6650, https://doi.org/10.5194/amt-11-6627-2018, 2018.

Fu, G., Hasekamp, O., Rietjens, J., Smit, M., Di Noia, A., Cairns, B., Wasilewski, A., Diner, D., Seidel, F., Xu, F., Knobelspiesse, K., Gao, M., da Silva, A., Burton, S., Hostetler, C., Hair, J., and Ferrare, R.: Aerosol retrievals from different polarimeters during the ACEPOL campaign using a common retrieval algorithm, Atmospheric Measurement Techniques, 13, 553–573, https://doi.org/10.5194/amt-13-553-2020, 2020.

https://doi.org/10.5194/egusphere-2026-6048
Preprint. Discussion started: 17 November 2026
© Author(s) 2026. CC BY 4.0 License.

Fu, G., Rietjens, J., Laasner, R., van der Schaaf, L., van Hees, R., Yuan, Z., van Diedenhoven, B., Hannadige, N., Landgraf, J., Smit, M., Knobelspiesse, K., Cairns, B., Gao, M., Franz, B., Werdell, J., and Hasekamp, O.: Aerosol Retrievals From SPEXone on the NASA PACE Mission: First Results and Validation, Geophysical Research Letters, 52, e2024GL113 525, https://doi.org/10.1029/2024GL113525, 2025.

Fu, G., Lu, S., Gao, M., Rietjens, J., and Hasekamp, O.: Collaborative Neural Networks Significantly Improve Global Aerosol Retrievals From Multiangle Polarimeters, IEEE Transactions on Geoscience and Remote Sensing, 64, 4107 019–4107 019, https://doi.org/10.1109/TGRS.2026.3685881, 2026.

Hasekamp, O., Litvinov, P., Fu, G., Chen, C., and Dubovik, O.: Algorithm evaluation for polarimetric remote sensing of atmospheric aerosols, Atmospheric Measurement Techniques, 17, 1497–1525, https://doi.org/10.5194/amt-17-1497-2024, 2024.

Hasekamp, O. P., Litvinov, P., and Butz, A.: Aerosol properties over the ocean from PARASOL multiangle photopolarimetric measurements, Journal of Geophysical Research: Atmospheres, 116, https://doi.org/10.1029/2010JD015469, 2011.

Hasekamp, O. P., Fu, G., Rusli, S. P., Wu, L., Di Noia, A., Brugh, J. a. d., Landgraf, J., Martijn Smit, J., Rietjens, J., and van Amerongen, A.: Aerosol measurements by SPEXone on the NASA PACE mission: expected retrieval capabilities, Journal of Quantitative Spectroscopy and Radiative Transfer, 227, 170–184, https://doi.org/10.1016/j.jqsrt.2019.02.006, 2019.

Holben, B. N., Eck, T. F., Slutsker, I., Smirnov, A., Sinyuk, A., Schafer, J., Giles, D., and Dubovik, O.: Aeronet's Version 2.0 quality assurance criteria, in: Remote Sensing of the Atmosphere and Clouds, vol. 6408, pp. 134–147, SPIE, https://doi.org/10.1117/12.706524, 2006.

Knobelspiesse, K., Barbosa, H. M. J., Bradley, C., Bruegge, C., Cairns, B., Chen, G., Chowdhary, J., Cook, A., Di Noia, A., van Diedenhoven, B., Diner, D. J., Ferrare, R., Fu, G., Gao, M., Garay, M., Hair, J., Harper, D., van Harten, G., Hasekamp, O., Helmlinger, M., Hostetler, C., Kalashnikova, O., Kupchock, A., Longo De Freitas, K., Maring, H., Martins, J. V., McBride, B., McGill, M., Norlin, K., Puthukkudy, A., Rheingans, B., Rietjens, J., Seidel, F. C., da Silva, A., Smit, M., Stamnes, S., Tan, Q., Val, S., Wasilewski, A., Xu, F., Xu, X., and Yorks, J.: The Aerosol Characterization from Polarimeter and Lidar (ACEPOL) airborne field campaign, Earth System Science Data, 12, 2183–2208, https://doi.org/10.5194/essd-12-2183-2020, 2020.

Knobelspiesse, K., Cairns, B., Cetinic, I., Ahern, A., Bennett, J. R., Bucholtz, A., Hair, J., Jordan, C., Martins, V., Meyer, K., Schlosser, J., Thompson, D., van Diedenhoven, B., and Ziemba, L.: Plankton, Aerosol, Cloud, ocean Ecosystem - Postlaunch Airborne eXperiment Campaign Data [Dataset], https://doi.org/10.5067/SUBORBITAL/PACE-PAX/DATA001, 2025a.

Knobelspiesse, K., Cairns, B., Cetinić, I., and LeBlanc, S.: The PACE Postlaunch Airborne eXperiment (PACE-PAX): post campaign report, National Aeronautics and Space Administration, Technical Memo 20250011273, NASA Technical Reports Server, https://doi.org/10.64631/IYHT2608, 2025b.

Knobelspiesse, K. D., Alfter, J., Cairns, B., Cetinić, I., LeBlanc, S., Nicholas, S., and Ueyama, R.: Field Campaign Design and Implementation with Traceability Matrix Decision Suppor, American Meteorological Society, 43, 133–148, https://doi.org/doi.org/10.1175/JTECH-D-25-0079.1, 2026.

Lu, S., Landgraf, J., Fu, G., van Diedenhoven, B., Wu, L., Rusli, S. P., and Hasekamp, O. P.: Simultaneous Retrieval of Trace Gases, Aerosols, and Cirrus Using RemoTAP—The Global Orbit Ensemble Study for the CO2M Mission, Frontiers in Remote Sensing, Volume 3 - 2022, https://doi.org/10.3389/frsen.2022.914378, 2022.

NASA Ocean Biology Processing Group: PACE SPEXone Level-1C Science Data, version 3, https://doi.org/10.5067/PACE/SPEXONE/L1C/SCI/3, 2025a.

NASA Ocean Biology Processing Group: PACE SPEXone Level-2 Regional Aerosol Optical Properties Over Land, RemoTAP Algorithm, version 3.0, https://doi.org/10.5067/PACE/SPEXONE/L2/AER_RTAPLAND/3.0, 2025b.

https://doi.org/10.5194/egusphere-2026-6048
Preprint. Discussion started: 17 November 2026
© Author(s) 2026. CC BY 4.0 License.

NASA Ocean Biology Processing Group: PACE SPEXone Level-2 Regional Aerosol Optical Properties Over Ocean, RemoTAP Algorithm, version 3.0, https://doi.org/10.5067/PACE/SPEXONE/L2/AER_RTAPOCEAN/3.0, 2025c.

Petters, M. D. and Kreidenweis, S. M.: A single parameter representation of hygroscopic growth and cloud condensation nucleus activity, Atmospheric Chemistry and Physics, 7, 1961–1971, https://doi.org/10.5194/acp-7-1961-2007, 2007.

Popp, T., De Leeuw, G., Bingen, C., Brühl, C., Capelle, V., Chedin, A., Clarisse, L., Dubovik, O., Grainger, R., Griesfeller, J., Heckel, A., Kinne, S., Klüser, L., Kosmale, M., Kolmonen, P., Lelli, L., Litvinov, P., Mei, L., North, P., Pinnock, S., Povey, A., Robert, C., Schulz, M., Sogacheva, L., Stebel, K., Stein Zweers, D., Thomas, G., Tilstra, L. G., Vandenbussche, S., Veefkind, P., Vountas, M., and Xue, Y.: Development, Production and Evaluation of Aerosol Climate Data Records from European Satellite Observations (Aerosol_cci), Remote Sensing, 8, 421, https://doi.org/10.3390/rs8050421, 2016.

Rietjens, J., Smit, M., Campo, J., Bouchan, T., Cooney, R., Piron, P., Tol, P., Laasner, R., van Hees, R., Landgraf, J., and Hasekamp, O.: SPEXone multi-angle spectropolarimeter characterization, calibration, and key data derivation using the L0-1B processor, in: International Conference on Space Optics — ICSO 2022, SPIE, https://doi.org/10.1117/12.2690892, 2023.

Rietjens, J. H. H.: Optical and system performance of SPEXone, a multi-angle channeled spectropolarimeter for the NASA PACE mission, in: International Conference on Space Optics — ICSO 2020, vol. 11852, SPIE, https://doi.org/10.1117/12.2690835, 2020.

Schlosser, J. S., Stamnes, S., Burton, S. P., Cairns, B., Crosbie, E., Van Diedenhoven, B., Diskin, G., Dmitrovic, S., Ferrare, R., Hair, J. W., Hostetler, C. A., Hu, Y., Liu, X., Moore, R. H., Shingler, T., Shook, M. A., Thornhill, K. L., Winstead, E., Ziemba, L., and Sorooshian, A.: Polarimeter + Lidar–Derived Aerosol Particle Number Concentration, Frontiers in Remote Sensing, 3, https://doi.org/10.3389/frsen.2022.885332, 2022.

Schlosser, J. S., Dmitrovic, S., Bennett, R., Cairns, B., Chen, G., Diskin, G. S., Ferrare, R. A., Hair, J. W., Jones, M. A., Reid, J. S., Shingler, T. J., Shook, M. A., Sorooshian, A., Thornhill, K. L., Ziemba, L. D., and Stamnes, S.: Closing the gap: an algorithmic approach to reconciling in-situ and remotely sensed aerosol properties, Atmospheric Measurement Techniques, 18, 7187–7220, https://doi.org/10.5194/amt-18-7187-2025, 2025.

Schuster, G. L., Lin, B., and Dubovik, O.: Remote sensing of aerosol water uptake, Geophysical Research Letters, 36, https://doi.org/10.1029/2008GL036576, 2009.

Sinyuk, A., Holben, B. N., Eck, T. F., Giles, D. M., Slutsker, I., Korkin, S., Schafer, J. S., Smirnov, A., Sorokin, M., and Lyapustin, A.: The AERONET Version 3 aerosol retrieval algorithm, associated uncertainties and comparisons to Version 2, Atmospheric Measurement Techniques, 13, 3375–3411, https://doi.org/10.5194/amt-13-3375-2020, 2020.

Smit, J. M., Rietjens, J. H. H., van Harten, G., Noia, A. D., Laauwen, W., Rheingans, B. E., Diner, D. J., Cairns, B., Wasilewski, A., Knobelspiesse, K. D., Ferrare, R., and Hasekamp, O. P.: SPEX airborne spectropolarimeter calibration and performance, Appl. Opt., 58, 5695–5719, https://doi.org/10.1364/AO.58.005695, 2019.

Smit, M., Rietjens, J., Campo, J., aan de Brugh, J., van Amerongen, A., Hasekamp, O., Landgraf, J., and Liu, X.: Polarimetric calibration of a spectro-polarimeter for remote sensing and characterization of aerosols, in: International Conference on Space Optics — ICSO 2020, edited by Cugny, B., Sodnik, Z., and Karafolas, N., vol. 11852, p. 1185232, International Society for Optics and Photonics, SPIE, https://doi.org/10.1117/12.2599475, 2021.

Snik, F., Karalidi, T., and Keller, C. U.: Spectral modulation for full linear polarimetry, Appl. Opt., 48, 1337–1346, https://doi.org/10.1364/AO.48.001337, 2009.

van der Schaaf, L., Jonker, M., Laasner, R., Rietjens, J., Hasekamp, O., Vretenar, M., Tol, P., and Smit, M.: Georegistration and viewport coregistration for SPEXone, the multi-angle spectropolarimeter on-board the NASA PACE satellite, in: Sensors, Systems, and Next-

https://doi.org/10.5194/egusphere-2026-6048
Preprint. Discussion started: 17 November 2026
© Author(s) 2026. CC BY 4.0 License.

Generation Satellites XXVIII, edited by Babu, S. R., Hélière, A., and Kimura, T., vol. 13192, p. 131920I, International Society for Optics and Photonics, SPIE, https://doi.org/10.1117/12.3031741, 2024.

van Diedenhoven, B., Hasekamp, O. P., Cairns, B., Schuster, G. L., Stamnes, S., Shook, M., and Ziemba, L.: Remote sensing of aerosol water fraction, dry size distribution and soluble fraction using multi-angle, multi-spectral polarimetry, Atmospheric Measurement Techniques, 15, 7411–7434, https://doi.org/10.5194/amt-15-7411-2022, 2022.

Wehr, T., Kubota, T., Tzeremes, G., Wallace, K., Nakatsuka, H., Ohno, Y., Koopman, R., Rusli, S., Kikuchi, M., Eisinger, M., Tanaka, T., Taga, M., Deghaye, P., Tomita, E., and Bernaerts, D.: The EarthCARE mission – science and system overview, Atmospheric Measurement Techniques, 16, 3581–3608, https://doi.org/10.5194/amt-16-3581-2023, 2023.

Werdell, P. J., Behrenfeld, M. J., Bontempi, P. S., Boss, E., Cairns, B., Davis, G. T., Franz, B. A., Gliese, U. B., Gorman, E. T., Hasekamp, O., Knobelspiesse, K. D., Mannino, A., Martins, J. V., McClain, C. R., Meister, G., and Remer, L. A.: The Plankton, Aerosol, Cloud, Ocean Ecosystem Mission: Status, Science, Advances, Bulletin of the American Meteorological Society, 100, 1775 – 1794, https://doi.org/10.1175/BAMS-D-18-0056.1, 2019.

Yuan, Z., Fu, G., van Diedenhoven, B., Lin, H. X., Erisman, J. W., and Hasekamp, O. P.: Cloud detection from multi-angular polarimetric satellite measurements using a neural network ensemble approach, Atmospheric Measurement Techniques, 17, 2595–2610, https://doi.org/10.5194/amt-17-2595-2024, 2024.

Ziemba, L. D., Lee Thornhill, K., Ferrare, R., Barrick, J., Beyersdorf, A. J., Chen, G., Crumeyrolle, S. N., Hair, J., Hostetler, C., Hudgins, C., Obland, M., Rogers, R., Scarino, A. J., Winstead, E. L., and Anderson, B. E.: Airborne observations of aerosol extinction by in situ and remote-sensing techniques: Evaluation of particle hygroscopicity, Geophysical Research Letters, 40, 417–422, https://doi.org/10.1029/2012GL054428, 2013.